

Judged by your neighbors: A novel framework for personalized assessment of brain structural aging effects in diverse populations

Ramona Leenings^{1,2,3*}, Nils R. Winter³, Jan Ernsting^{3,4},
Maximilian Konowski³, Vincent Holstein^{5,6,7}, Susanne Meinert³,
Jennifer Spanagel³, Carlotta Barkhau³, Lukas Fisch³,
Janik Goltermann³, Malte F. Gerdels³, Dominik Grotegerd³,
Elisabeth J. Leehr³, Annette Peters^{8,9,10,11}, Lilian Krist¹²,
Stefan N. Willich¹², Tobias Pischon¹³, Henry Völzke^{14,15},
Johannes Haubold^{16,17}, Hans-Ulrich Kauczor¹⁸, Thoralf Niendorf¹⁹,
Maike Richter²⁰, Udo Dannlowski³, Klaus Berger²¹, Xiaoyi Jiang¹,
James Cole^{22,24}, Nils Opel^{2,24,25†}, Tim Hahn^{3†}, for the NAKO
consortium^a, the ADNI consortium^b, the Frontotemporal Lobar
Degeneration Neuroimaging Initiative^c, the Australian Imaging
Biomarkers and Lifestyle flagship study of ageing^d

^a Data used in the preparation of this article were obtained from the German National Cohort (NAKO) (www.nako.de). The NAKO is funded by the Federal Ministry of Education and Research (BMBF) [project funding reference numbers: 01ER1301A/B/C, 01ER1511D, 01ER1801A/B/C/D and 01ER2301A/B/C], federal states of Germany and the Helmholtz Association, the participating universities and the institutes of the Leibniz Association. NAKO researchers are listed in the acknowledgements.

^b Data used in the preparation of this article were obtained from the Alzheimer's Disease Neuroimaging Initiative (ADNI) database (adni.loni.usc.edu). The ADNI was launched in 2003 as a public-private partnership, led by Principal Investigator Michael W. Weiner, MD. The primary goal of ADNI has been to test whether serial magnetic resonance imaging (MRI), positron emission tomography (PET), other biological markers, and clinical and neuropsychological assessment can be combined to measure the progression of mild cognitive impairment (MCI) and early Alzheimer's disease (AD).

^c Data used in preparation of this article were obtained from the Frontotemporal Lobar Degeneration Neuroimaging Initiative (FTLDNI) database. The investigators at NIFD/FTLDNI contributed to the design and implementation of FTLDNI and/or provided data, but did not participate in analysis or writing of this report (unless otherwise listed). FTLDNI researchers are further listed in the acknowledgment section.

^d Data used in the preparation of this article was obtained from the Australian Imaging Biomarkers and Lifestyle flagship study of ageing (AIBL) funded by the Commonwealth Scientific and Industrial Research Organisation (CSIRO) which was made available at the ADNI database (www.loni.usc.edu/ADNI). The AIBL researchers contributed data but did not participate in analysis or writing of this report. AIBL researchers are listed at www.aibl.csiro.au.

¹Faculty of Mathematics and Computer Science, University of Münster,
Münster, Germany.

²Department of Psychiatry and Psychotherapy, Jena University
Hospital, Jena Germany.

³University of Münster, Institute of Translational Psychiatry, Münster
Germany.

⁴Institute for Geoinformatics, University of Münster, Münster Germany.
⁵McLean Hospital, Belmont USA.

⁶Department of Psychiatry, Harvard Medical School, Boston USA.

⁷Stanley Center for Psychiatric Research, Broad Institute of MIT and
Harvard, Cambridge USA.

⁸Institute of Epidemiology, Helmholtz Zentrum München, German
Research Center for Environmental Health (GmbH), Neuherberg,
Germany.

⁹Chair of Epidemiology, Institute for Medical Information Processing,
Biometry and Epidemiology, Ludwig-Maximilians-Universität München,
Munich, Germany.

¹⁰German Center for Diabetes Research (DZD e.V.), Neuherberg,
Germany.

¹¹German Center for Mental Health (DZPG), partner site Munich,
Munich, Germany.

¹²Institute of Social Medicine, Epidemiology and Health Economics,
Charité - Universitätsmedizin Berlin, Berlin, Germany.

¹³Molecular Epidemiology Research Group, Max Delbrück Center for
Molecular Medicine in the Helmholtz Association (MDC), Berlin,
Germany.

¹⁴German Centre for Cardiovascular Research (DZHK), Greifswald,
Germany.

¹⁵Institute for Community Medicine, University Medicine Greifswald,
Greifswald, Germany.

¹⁶Institute of Diagnostic and Interventional Radiology and
Neuroradiology, University Hospital Essen, Essen, Germany.

¹⁷Institute for Artificial Intelligence in Medicine (IKIM), University
Hospital Essen, Essen, Germany.

¹⁸Diagnostic and Interventional Radiology, University Hospital
Heidelberg, Heidelberg, Germany.

¹⁹Berlin Ultrahigh Field Facility, Max Delbrück Center for Molecular
Medicine in the Helmholtz Association (MDC), Berlin, Germany.

²⁰Department of Psychiatry and Psychotherapy, Charité –
Universitätsmedizin Berlin, Berlin, Germany.

²¹Institute of Epidemiology and Social Medicine, University of Münster, Münster, Germany.

²²Department of Computer Science, Centre for Medical Image Computing, University College London, London, United Kingdom.

²³Dementia Research Centre, Institute of Neurology, University College London, London, United Kingdom.

²⁴ German Center for Mental Health (DZPG), Jena-Magdeburg-Halle, Germany.

²⁵ Center for Intervention and Research on adaptive and maladaptive brain Circuits underlying mental health (C-I-R-C)Germany, Jena-Magdeburg-Halle, Germany.

*Corresponding author(s). E-mail(s): leenings@uni-muenster.de;

†These authors contributed equally to this work.

Abstract

Despite their promise, current neuroimaging biomarkers often fail to capture the full spectrum of inter-individual variability in brain structure and aging effects. This limits their ability to detect subtle norm deviations and impacts their utility for personalized care. We introduce Nearest Neighbor Normativity (N³), a novel framework designed to resolve the confound between natural diversity and subtle pathological patterns. It evaluates individual brain structures from several meaningful viewpoints, accommodates a variety of co-existing normative prototypes and accounts for individually varying progression rates of brain structural decline. Using MRI data of 36,896 individuals, we provide empirical evidence that the N³ biomarker effectively disentangles natural inter-individual variability from pathological alterations, significantly outperforming brain age models and traditional normative modeling approaches in the detection of neurodegenerative diseases. The N³ framework is easily adaptable to various medical domains, fostering individualized and context-rich biomarkers and paving the way for more targeted and personalized therapeutic strategies.

Keywords: Normative Modeling, Precision Medicine, Diversity, Brain Age, Density-Estimation

1 Introduction

- ¹ Neuroimaging biomarkers hold the promise to transform psychiatric research by providing objective measures that can move the field beyond symptom descriptions [1–6].
- ³ Neuroimaging biomarkers are closely tied to the concept of brain structural normativity, i.e. the degree of alignment with expected norms seen in the general population.
- ⁵ Despite established consensus about the individuality in brain structure, current

6 biomarker assessments heavily rely on population averages and inherently exclude
7 the possibility of multiple, equally viable normative patterns. The pursue of precision
8 medicine requires to shift away from group averages and tailor medical interventions
9 to individual physiology [7, 8]. In fact, finding (subtle) individual anomalies moder-
10 ates our ability to diagnose and treat diseases effectively and is a practical necessity
11 for the personalization of patient care. Redefining neuroimaging biomarkers to better
12 account for the population-inherent diversity is thus not merely an academic exercise,
13 but holds profound implications for medical practice.

14 Two prominent approaches have emerged in the search for reliable neuroimaging
15 biomarkers in brain structure thus far. The first approach, called Brain Age [9, 10],
16 trains machine learning models to predict chronological age from brain structure using
17 examples of a healthy reference sample. The goal is to detect unusual brain structural
18 decline in unseen samples. The resulting biomarker, the Brain Age Gap (BAG), is
19 defined as the difference between chronological and predicted age and has been sta-
20 tistically associated with numerous neurological and psychiatric conditions, such as
21 Alzheimer's Disease (+5-10 years), Mild Cognitive Impairment, (+1-10 years), Major
22 Depressive Disorder (BAG 1-4 years), Schizophrenia (+3-12 years). [11-15].

23 However, the BAG's ability to capture individual norm deviations is naturally
24 limited due to the multifaceted nature of individual aging processes. How quickly
25 aging effects progress in individuals is highly variable and a complex interplay of
26 genetic predisposition, behavioral choices and cumulative impact of various adverse
27 or protective exposures [16-20]. This unique combination of factors inevitably results
28 in different aging effects seen among same-aged individuals. Using chronological age
29 to assess normative neurodegeneration thus inherently lacks precision. Consequently,
30 the resolution of the BAG as a personalized brain structural assessment tool is limited
31 and its utility mainly constrained to group comparisons.

32 The second prominent approach towards a brain structural biomarker emerges from
33 so-called normative modeling [21]. Normative modeling uses statistical distributions
34 to quantify brain structural measures in relation to the population average and the
35 variance around it [22]. It has been successfully applied to detect brain structural
36 norm deviations in various psychiatric disorders [23]. By design, normative models
37 interpolate natural variability into a single reference distribution, centered around
38 the population average. This mean-centric framework neglects the heterogeneity of
39 physiological manifestations and does not account for biologically valid alternative
40 norms. Thus, these population-wide, and often univariate, models risk masking subtle
41 details that are critical for obtaining nuanced individual clinical insights [24].

42 To address the methodological shortcomings of the approaches described above,
43 we propose a novel normativity estimation framework called Nearest Neighbor Nor-
44 mativity (N³). It uses four core strategies to better understand an individual brain
45 structure within the natural diversity of the population.

46 *Demographic contextualization.*

47 First, it evaluates brain structures in relation to demographically matched subgroups
48 to reduce confounding variability. We hypothesize that this narrower comparison
49 enables the detection of nuanced deviations often overlooked in broader models.

50 **Multinorm accommodation.**

51 Second, the N³ framework avoids comparisons to the population average and instead
52 accommodates a variety of normative brain structural prototypes per age-group.
53 Methodologically, this can be expressed with straightforward and distribution-free
54 local density estimation techniques such as the Nearest Neighbor Algorithm [25].

55 **Normativity profiles.**

56 Third, each individual receives a so-called normativity profile, which joins multiple
57 evaluations from different meaningful viewpoints into an comprehensive overview. In
58 particular, it quantifies how an individual's brain structure aligns with expected pat-
59 terns across the aging continuum, positioning it within the spectrum of aging effects
60 (see Figure 2).

61 **Clinically adaptable metric.**

62 Fourth, an analysis of the normativity profile distills its context into a single metric
63 which we call the N³ biomarker. The N³ biomarker expresses how common a norma-
64 tivity profile appears in relation to a particular clinical subgroup. In this work, we use
65 the N³ biomarker to express the typicality of aging effects seen in an individual brain
66 structure for a particular age group. Nevertheless, clinicians can adapt this metric to
67 specific goals, for example, to identify typical profiles associated with high treatment
68 response.

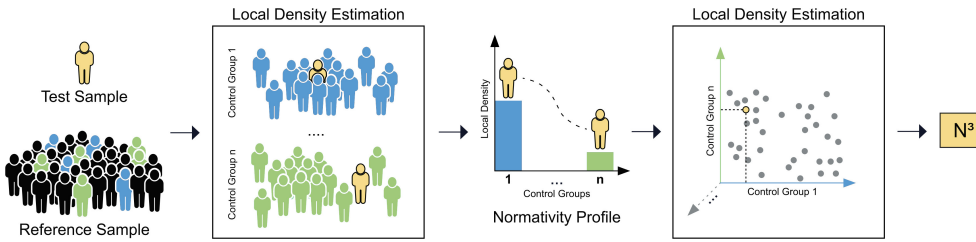


Fig. 1 Our proposed N³ framework entails methodological innovations that refine normativity assessments in large and diverse medical datasets. Here, we apply it to brain structure to foster the detection of pathological norm deviations amidst neuroanatomical variability and individual progression rates in aging-related decline. The N³ entails four key strategies. First, we propose to use several carefully tailored control groups to promote the detection of subtle and nuanced anomalies that may escape broader comparative models. Second, we refrain from comparisons to a single normative tendency such as the population average. Instead, we propose to quantify normativity assessment with local density estimation algorithms, which effectively embraces diversity and acknowledges the possibility of multiple, equally viable health states in the population. Third, we introduce global context to the normativity assessments and join multiple comparative normativity estimations per individual into a so-called normativity profile. This normativity profile acts as a holistic representation of a patient's health status and provides a multifaceted contextualization to the complex and heterogeneous nature of medical observations. Fourth, we convert the normativity profile into a singular, actionable metric, which we call N³. It synthesizes the accumulated information of prior steps and can be adapted to a variety of clinical inquiries. For example, the final N³ normativity assessment can be fine-tuned to express normativity in relation to specific clinical outcomes. In the example of brain structure, normativity profiles can for example be compared to those of patients who exhibit high treatment response. The N³ approach is universally applicable, and we see great potential that its application will advance normativity assessments and contribute to personalized patient care.

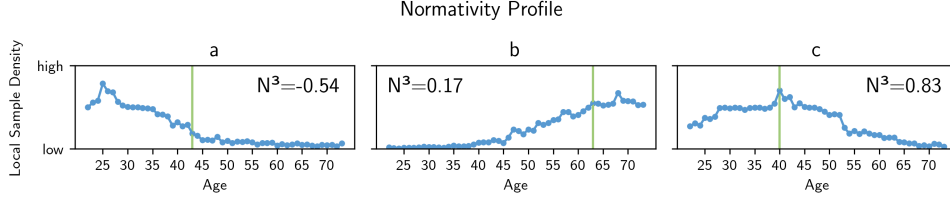


Fig. 2 Individual brain structural normativity profiles of three exemplary individuals of the training sample (see Methods 1 and 2). The normativity profile shows a brain structure's level of coherence with different reference samples along the age continuum (blue). Chronological age is depicted in green. The N^3 framework compares aging effects of a particular brain structure to expected aging patterns of different age groups along the age continuum. Moreover, the use of local density estimation technique enables several normative prototypical brain structures per age bin and is able to capture varying, yet normative rates of aging-related decline. a) An individual's brain structure aligns with younger brain structures, indicating fewer aging effects as commonly seen in same-aged individuals b) An individual brain structure aligns with older brain structures, indicating premature neurodegeneration processes. c) A brain structure exhibits high alignment within its own age group and shows deprecating alignment within other age groups.

69 In summary, the N^3 approach addresses a key concern in neurological research,
70 namely the challenge of distinguishing inter-individual variability in healthy brain
71 structural decline from pathological norm deviations. By providing a more comprehen-
72 sive and context-rich assessment of individual brain structures, the N^3 is inherently
73 designed to improve the understanding of neuroanatomical diversity and the detection
74 of unusual patterns. We benchmark the efficacy of the N^3 framework relative to con-
75 ventional neuroimaging biomarkers. To this end, we use neurodegenerative diseases as
76 model diseases to represent brain structural alterations and pathological norm devia-
77 tions. We show that, indeed, the N^3 biomarker enables enhanced understanding of the
78 heterogeneous and complex neuroanatomical variability and individual pathological
79 norm deviations.

80 2 Results

81 All normative models are trained with neuroimaging data from T1-weighted MRI
82 scans of 29,883 individuals of a large population-based study and evaluated in 7,013
83 individuals with varying levels of neurodegeneration from different study populations
84 (see Methods 2). Our analysis focuses on gray matter (GM), white matter (WM),
85 hyperintense white matter (WMH), total intracranial volume (TIV) and cerebrospinal
86 fluid (CSF) volumes. These global measures provide a comprehensive overview of
87 brain structure[26]. We use these broad aggregates of complex physiological features
88 to represent typical clinical measurements, and verify the algorithm's efficacy to derive
89 meaningful disease indicators from these global parameters.

90 We evaluate the N^3 marker efficacy against conventional normative modeling
91 approaches. Using classical normative modeling [21, 23], we derive two normativity
92 scores, the first being the sum of the absolute z-scores (NM-S), the second counting
93 the number of z-scores whose magnitude deviates beyond a threshold of ± 1.96 (NM-
94 C). We also benchmark our approach against the Brain Age paradigm, which utilizes a

95 machine learning model to predict chronological age from brain structural data[9, 11].
96 Deviations between predicted and actual age, referred to as the Brain Age Gap (BAG)
97 indicate neurodegenerative alterations (for details please refer to Methods Section 1,
98 3 and 4)

99 Applying the normative models to evaluate brain structure of both cognitively
100 healthy and diseased individuals, we validate the ability of each biomarker to differ-
101 entiate between healthy inter-individual variability and (early) states of pathological
102 decline. To this end, instances of Mild Cognitive Impairment (MCI), Alzheimer's Dis-
103 ease (AD) and Frontotemporal Dementia (FTD) serve as model diseases to represent
104 brain structural alterations and pathological norm deviations.

105 **2.1 Increased statistical explanatory power in distinguishing 106 neurodegenerative diseases**

107 First, we assessed the statistical power of each biomarker, specifically examining the
108 extent to which the marker detects unusual pattern deviations in group-level analyses.
109 We calculated the effect size (partial eta squared, η^2) for the classification of healthy
110 individuals from those affected by disease (MCI, AD or FTD, respectively; see Meth-
111 ods 5.5). Post-hoc comparisons then enabled us to evaluate which biomarker was able
112 to provide the most statistical power. The N³ marker consistently showed higher dis-
113 criminative ability across all neurodegenerative conditions compared to other markers
114 used in the study (see Figure 3 and Table 1).

115 For AD, the N³ biomarker showed the largest effect size ($\eta^2 = 0.29$), signifying that
116 approximately 29% of the variability can be explained by differences in the N³ marker
117 levels between the AD group and controls. In the context of FTD, all markers demon-
118 strated large effect sizes, while the N³ stood out with an effect size of $\eta^2 = 0.38$. The
119 results for Mild Cognitive Impairment (MCI) differed, as all markers showed generally
120 lower explanatory power. Nonetheless, the N³ marker displayed a relative advantage,
121 with an effect size of $\eta^2 = 0.07$, compared to $\eta^2 = 0.05$ for the Brain Age Gap (BAG)
122 and $\eta^2 = 0.02$ for the normative modeling scores. Overall, the results suggest N³'s
123 enhanced capability of discerning the subtle and complex neurostructural alterations
124 associated with different stages of pathological decline in group level analysis.

125 **2.2 Improved personalized predictions**

126 Second, we conduct machine learning analyses to evaluate each biomarker's util-
127 ity in predicting the occurrence of a neurodegenerative disease on a single-subject
128 level. Machine learning models transcend conventional statistical models by handling
129 multivariate and non-linear relationships and shifting the focus from group average
130 comparisons to predictions on an individual level[27]. We employ cross-validation
131 strategies, which systematically tests each marker against new, unseen data to verify
132 the accuracy, robustness, and generalizability of the models. Such validation is imper-
133 ative to ensure reliability when these markers are applied in clinical environments [28].
134 The performance of the machine learning models is quantitatively evaluated using met-
135 rics such as sensitivity, precision, balanced accuracy, and the F1-score —each providing
136 a different lens through which to assess clinical utility. Balanced accuracy provides a

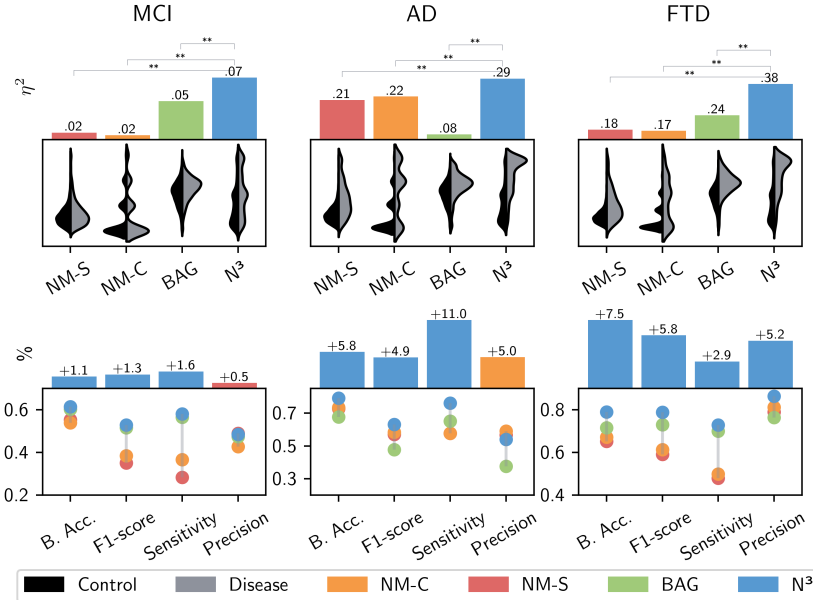


Fig. 3 **Top:** The top panel shows the results of the statistical analyses. Statistical effect sizes (partial eta squared - η^2) are given for the different biomarkers (N^3 - our approach, NM-S - the sum of the absolute z-scores, NM-C - the number of z-scores whose magnitude deviates beyond a threshold of ± 1.96 , and the BAG - Brain Age Gap). We evaluate each normative modeling approach's ability to parse inter-individual variability and detect pathological alterations. For each marker, we test the ability to differentiate between controls and diseased individuals in group-level analyses, using neurodegenerative diseases as representative models of adverse norm deviations and pathological patterns. Results are given for Mild Cognitive Impairment (MCI), Alzheimer's Disease (AD), and Frontotemporal Dementia (FTD), respectively. Post-hoc comparisons of the effect sizes revealed larger explained variance of our N^3 marker in all neurodegenerative conditions. The level of significance in the differences between the η^2 of N^3 and η^2 of the other normativity estimation approaches is indicated above. Significance was confirmed through permutation testing using 1000 random permutations. The distribution plots below show each marker's value distributions for healthy controls (black) and diseased individuals (gray). **Bottom:** We use machine learning to evaluate the expressiveness of each biomarker on a single-subject level. The N^3 marker demonstrated increased accuracy in predicting the occurrence of pathological norm deviations, in this case the presence of neurodegenerative diseases for individual patients. We show the different marker's performance metrics [balanced accuracy (B.Acc), F1-Score, Recall and Precision] and the performance advantage of the best marker in relation to the second best marker in percentage (above).

137 holistic view, ensuring that both the presence and absence of disease are accurately
 138 identified. Sensitivity is particularly critical in a clinical setting as it measures the
 139 model's capability to capture as many diseased patients as possible, thus effectively
 140 measuring a biomarker's utility as a screening tool. Complementary precision ensures
 141 that the majority of patients identified by the model as having a disease truly have
 142 the disease. The F1-score is crucial for its balance of precision and sensitivity—a vital
 143 feature to avoid unnecessary interventions or over-treatment or unnecessary expensive
 144 screening programs.

145 The findings, as presented in Figure 3 and Table 1, elucidate the efficacy of the
146 N³ marker across various disorders. In the specific cases of AD and FTD, the N³
147 marker demonstrated notable improvements in balanced accuracy scores—surpassing
148 the second-best markers by 5.8% for AD and 7.5% for FTD. However, in alignment
149 with the small effect sizes observed in statistical analysis, the efficacy of all markers
150 notably declined in predicting the presence of MCI from the given variables. Here, the
151 N³ reached an 1.1% improvement to the next best marker, the BAG. With regard to
152 the F1-scores, the N³ marker achieved the highest performance in all neurodegener-
153 ative diseases, demonstrating its adeptness at balancing sensitivity and precision in
154 detecting disease cases. While N³'s precision for MCI was 0.5% behind the normative
155 modeling marker (NM-S) and by 5.0% in AD (NM-C), it was superior by 5.2% for
156 FTD compared to the second best result (NM-C). Moreover, the N³ marker displayed
157 superior sensitivity rates in all conditions (+1.6%, +11.0% and +2.9%), highlighting
158 its sensitivity in identifying (subtle) neurodegenerative patterns. Given the overlap to
159 normative aging patterns and the individuality in disease manifestations, particularly
160 in MCI, this is a notable performance increase and indicates the N³ approach's utility
161 in decoding sparse associations. Overall, N³'s relative superiority over other markers
162 emphasizes its efficacy in differentiating inter-individual variability from pathological
163 variations in unseen individuals. The results provide evidence for the expressiveness
164 of the proposed N³ normative modeling approach, indicating its ability to parse inter-
165 individual heterogeneity effectively to evaluate individual measurements intricately
166 within the broader landscape of diverse medical data.

167 2.3 Stability and Robustness of the N³ marker

168 The calculation of the N³ marker relies on local density estimation. As such it is highly
169 dependent on the composition of the reference sample. Therefore, we investigate how
170 changes to the sample composition and sample size affect the stability of the N³ model.
171 We retrained N³ models with downsampled subsets of varying size, thereby mimicking
172 smaller studies and different study participants. We then apply the different normativity
173 models and predict normativity on an external dataset. Particularly, we evaluate if
174 predictions remain consistent across different sample sizes and sample compositions.
175 We quantify the stability of the normativity estimates by calculating the Intraclass
176 Correlation Coefficient (ICC) 18 (see Methods Section 5). Results are visualized in
177 Figure 4. We see that random samples of 200 individuals and above show consistently
178 high stability (ICC of 0.75 and above). Moreover, the ICC converges to excellent levels
179 (0.9 and above) in larger sample sizes, starting at 300 participants. While the results
180 are calculated for the use case of brain structural normativity estimation, they are a
181 first indication density-estimation based normative models can be realized by dividing
182 larger samples into subgroups of a few hundred samples and above.

183 Furthermore, it is essential for normativity estimations to remain consistent and
184 interpretable along the aging continuum, i.e., across different age groups, to avoid age
185 biases that could complicate both research and clinical interpretations. An analysis of
186 the age correlation of the N³ marker (presented in Figure 4a) indicates its stability
187 over the age range, showing no significant association to age. In comparison, tradi-
188 tional normative models show a significant but smaller correlation to age ($\rho=0.11-0.16$,

Table 1 Overview of the results achieved in statistical and machine learning analyses. To quantify the expressiveness of the different methodological approaches, we evaluate the different biomarkers' ability in distinguishing between normative inter-individual variability and pathological alterations. We report the effect size η^2 , representing the amount of variance explained by each of the different normativity markers in statistical group comparisons. We compare N³ - our approach, NM-S - the sum of the absolute z-scores, NM-C - the number of z-scores whose magnitude deviates beyond a threshold of ± 1.96 , and the BAG - Brain Age Gap for Mild Cognitive Impairment (MCI), Alzheimer's Disease (AD), and Frontotemporal Dementia (FTD), respectively. Moreover, we report the F-statistic, reflecting the relation of the marker variance between cognitive unimpaired and diseased individuals in relation to the respective intra-group variance, further indicating its ability to identify pathology in group-level analyses. All F-statistics and effect sizes η^1 are significant ($p < 0.001$). The performance results of the machine learning analyses are given, where the normativity markers are used to predict the occurrence of the neurodegenerative diseases in individual cases. The metrics provide insights into each marker's clinical utility, and overall efficacy in handling inter-individual variability and pathological variations across different neurodegenerative conditions on a single subject level. Highest performance is indicated in bold. We see that the N³ brain structural normativity marker shows relative superiority in relation to the other biomarkers, indicating the approach's efficacy in processing inter-individual variability and delineating potential anomalies.

Marker	F-statistic	Effect size η^2	B. Accuracy	F1-score	Sensitivity	Precision
Mild Cognitive Impairment (MCI)						
NM-C	$F(1,4565) = 74$	0.016	0.539 ± 0.010	0.385 ± 0.057	0.367 ± 0.090	0.427 ± 0.028
NM-S	$F(1,4565) = 85$	0.018	0.553 ± 0.013	0.352 ± 0.044	0.284 ± 0.070	0.490 ± 0.044
BAG	$F(1,4565) = 220$	0.046	0.603 ± 0.011	0.516 ± 0.014	0.566 ± 0.030	0.475 ± 0.016
N ³	$F(1,4565) = 326$	0.067	0.614 ± 0.011	0.529 ± 0.013	0.582 ± 0.023	0.485 ± 0.014
Alzheimer's Disease (AD)						
NM-C	$F(1,3709) = 1,073$	0.225	0.733 ± 0.020	0.583 ± 0.027	0.578 ± 0.047	0.591 ± 0.010
NM-S	$F(1,3709) = 994$	0.212	0.727 ± 0.023	0.570 ± 0.031	0.578 ± 0.057	0.567 ± 0.022
BAG	$F(1,3709) = 328$	0.081	0.676 ± 0.023	0.477 ± 0.025	0.651 ± 0.054	0.376 ± 0.014
N ³	$F(1,3709) = 1,529$	0.292	0.791 ± 0.020	0.632 ± 0.020	0.761 ± 0.049	0.541 ± 0.010
Frontotemporal Dementia (FTD)						
NM-C	$F(1,580) = 121$	0.173	0.671 ± 0.028	0.613 ± 0.043	0.499 ± 0.063	0.812 ± 0.073
NM-S	$F(1,580) = 125$	0.178	0.653 ± 0.042	0.592 ± 0.034	0.479 ± 0.047	0.790 ± 0.097
BAG	$F(1,580) = 184$	0.242	0.715 ± 0.076	0.731 ± 0.073	0.700 ± 0.073	0.765 ± 0.077
N ³	$F(1,580) = 348$	0.377	0.790 ± 0.063	0.789 ± 0.059	0.729 ± 0.063	0.864 ± 0.080

¹⁸⁹ p<0.001). This is a contrast to the Brain Age Gap (BAG), which exhibits a moderate age bias ($\rho=0.21$, p<0.001), even after bias correcting adjustments are made, (see ¹⁹⁰ Methods Section 3).

¹⁹¹ In terms of inter-marker relationships (detailed in Figure 4), the correlation analysis shows generally weak associations ($0.19 < |\rho| < 0.25$) among the various markers. ¹⁹² Two exceptions were noted: a strong correlation ($\rho=0.79$) between the two normative modeling markers — expected due to their derivation from the same normative ¹⁹³ models — and a moderate to strong correlation ($\rho=0.65$) between the BAG and the ¹⁹⁴ N³ marker. The correlations indicate underlying differences in what these markers are ¹⁹⁵ measuring about brain structural normativity, suggesting a potential for a combined ¹⁹⁶ utility in clinical settings.

¹⁹⁷ 3 Discussion

¹⁹⁸ We have introduced the N³ framework, which extends existing normative modeling ¹⁹⁹ approaches by accommodating a variety of normative population prototypes and evaluating ²⁰⁰ individuals from multiple comparative angles. We applied it to brain structure,

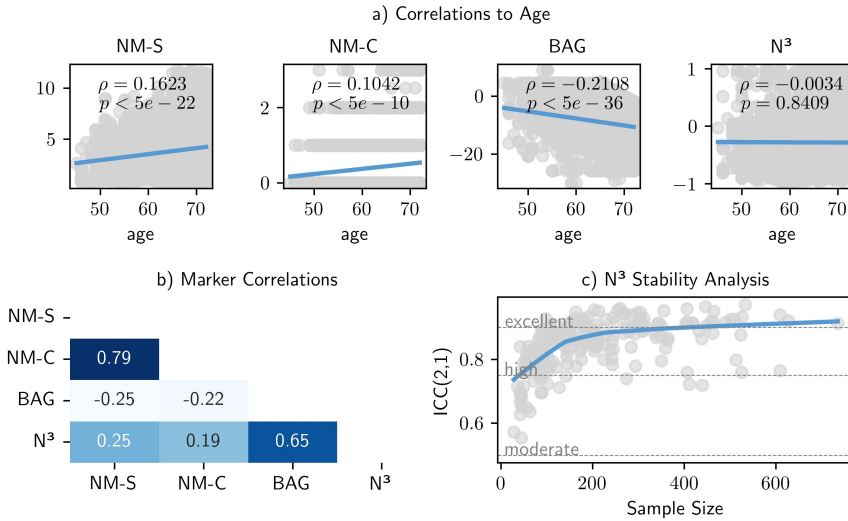


Fig. 4 Our evaluations revealed high robustness and consistency of the N^3 framework. a) We explored the age bias across different brain structural biomarkers in a healthy reference sample. In contrast to the other normativity estimation approaches, the N^3 marker showed no significant association to age, which allows a consistent interpretability across different age groups. b) Additionally, we calculated the correlation matrix among the different biomarkers, which emphasize the distinctiveness and complementarity of the N^3 marker. c) We tested the impact of sample size and sample composition on the reliability of the N^3 biomarker through intraclass correlation coefficients. To do so we repeatedly downsampled the training data to a random subset, mimicking smaller samples and different sample compositions. We see that the N^3 marker exhibits high stability (ICC of 0.75 and above) starting from small sample sizes of around 100 individuals and converges to excellent stability (ICC of 0.9 and above) in sample sizes of three hundred individuals and above.

204 which resulted in an informative biomarker assessing aging effects from multiple per-
 205 spectives along the aging continuum. Notably, the N^3 framework entails several layers
 206 of context while at the same time refining individual assessments. We provided evi-
 207 dence that the strategic alterations of the N^3 framework yield increased expressiveness
 208 and enabled superior differentiation between natural inter-individual variability and
 209 pathological alterations. In comparison to commonly used normativity scores and the
 210 widely referenced Brain Age approach, the N^3 marker showed increased efficacy in
 211 identifying pathological brain structural changes.

212 Notably, our evaluations are based on only five variables reflecting global brain
 213 structure volumes. As such, they are broad aggregates of complex physiological fea-
 214 tures and represent the character of many clinical measurements. In our application,
 215 the N^3 approach has demonstrated its ability to effectively decode the relevant infor-
 216 mation contained in these limited neurobiological variables and was able to extract
 217 meaningful insights.

218 Limitations of our proposed N^3 framework include its reliance on larger sample
 219 sizes, a factor not always feasible in clinical studies where resource efficiency dictates

220 smaller study populations. To maximize statistical power and mitigate the confounding
221 effects of clinical covariates, the heterogeneity in these smaller studies is often
222 restricted, which inadvertently limits their generalizability and applicability of out-
223 comes across the heterogeneous population [29, 30]. In our evaluations, the N^3 marker
224 exhibited high stability in samples of a few hundred individuals, indicating substantial
225 robustness in moderately-sized research study populations. Moreover, the N^3 marker
226 showed consistency across age groups, i.e., no correlation to age, which means that
227 its interpretation is consistent across individuals from different age groups and facil-
228 itates its interpretability in statistical analyses. Moreover, the framework's effectiveness
229 relies on the choice of a density estimation algorithm. In our application, the Nearest
230 Neighbor Algorithm depends on the k parameter, which defines the number of neigh-
231 bors considered in the estimation of the local sample density. In our approach, limiting
232 the number of neighbors to 10% with an upper bound to 15 prevented overly broad
233 comparisons while maintaining sufficient robustness across all control groups. In gen-
234 eral, the underlying algorithm can be customized for different scenarios, or adapted to
235 accommodate different medical data modalities, e.g., by using custom distance metrics
236 or dimensionality reduction techniques [31, 32].

237 We developed the N^3 approach in alignment to the goals of precision medicine.
238 A refined definition of reference values and population norms enhances our under-
239 standing of normative variability in diverse populations and fosters the detection of
240 individual pathological alterations [33–37]. As diversity and scale of datasets increase,
241 we need to reevaluate how population norms are derived, applied, and interpreted in
242 clinical practice [38–41]. The N^3 framework embraces the complexity in patient data,
243 contextualizes it against heterogeneous population standards and parses the diversity
244 into an interpretable and actionable metric.

245 The interpretation and contextualization of individual brain structures holds sig-
246 nificant potential for various domains. As stated above, a reliable biomarker for brain
247 structural normativity is eagerly sought in neuropsychiatric research. Here, biomarkers
248 may enable comprehensive assessments of neurostructural alterations associated with
249 specific symptoms, to better understand the etiology and pathogenesis of different dis-
250 ease phenotypes [24, 27, 42]. In general, a valid and robust neurostructural biomarker
251 would allow us to measure the impact of environmental factors, treatment options and
252 neuroinflammatory processes to understand disease mechanics and optimize individual
253 disease management strategies [12, 19, 43, 44].

254 In the realm of neurodegenerative diseases, the ability to detect brain struc-
255 tural alterations early is of critical clinical relevance, as it has been shown that
256 structural changes in the brain can manifest well before clinical symptoms become
257 apparent [45, 46]. Furthermore, evidence supports the presence of multiple underly-
258 ing neuropathological processes [17, 47], underscoring the methodological importance
259 for models accommodating multiple disease prototypes. Here, a reliable brain struc-
260 tural screening tool could be attached to routine MRI scans to promote early disease
261 interception and facilitate timely interventions that may prevent or delay disease pro-
262 gression [48–51]. To this end, we intend to extend our approach to process scans of
263 different MRI tissue contrasts and evaluate different deep-learning based embeddings

264 to optimize information gain. Moreover, we intend to investigate the resulting marker's
265 relation to genetic risk factors [52–55].

266 Our approach accommodates the multivariate nature of brain structures [56] and
267 aligns with other modern understandings of heterogeneity, such as the concept of
268 neurotypicality [57–59]. Traditionally seen as a uniform standard, brain architectures
269 are now understood to encompass a spectrum of neurological function and structures,
270 reflecting the rich diversity of the human nature. Moreover, our findings resonate with
271 recent work by Yang et al., where the authors found a range of multiple, co-occurring
272 patterns of brain aging [52]. Their research underscores the significant inter-individual
273 and also intra-individual variability, underscoring the complexity and uniqueness of
274 individual neurodegenerative processes beyond population averages.

275 As the critical role of individual norm deviations resonates through every facet
276 of personalized medicine, we aim to refine and expand our normativity estimation
277 approach to medical domains beyond brain structure. In general, the N³ framework
278 aligns well with the goals of precision medicine, offering a more personalized and
279 nuanced understanding of individual variability in aging or disease trajectories.

280 4 Conclusion

281 This approach that we call Nearest Neighbor Normativity (N³) interprets individual
282 patient data in reference to a particularly matched sample, accommodates diverse
283 population norms, and analyzes several different perspectives of normativity. Thereby,
284 it holds significant promise for personalized healthcare. It can be applied across various
285 medical domains to contextualize individual patient data in large and heterogeneous
286 datasets. As we continue to refine and validate our N³ framework, it is our belief
287 that the insights gained will be invaluable for shaping normativity assessments and
288 contribute to more personalized patient care and improved clinical outcomes.

289 5 Methods

290 5.1 N³ algorithm

291 The N³ approach is based on local density estimation in tailored control groups. To
292 establish a normative reference for the local density seen in a representative sample,
293 we here use the simple and intuitive Nearest-Neighbor algorithm [25, 32].

294 5.1.1 Local density estimation in tailored control groups

295 Let $X_c \in X$ be a control group of dataset X and $C = \{c_1, c_2, \dots, c_g\}$ be the
296 set of g control groups, where control groups are allowed to overlap. Each control
297 group X_c contains n samples $\{q_1, q_2, \dots, q_n\}$, which are characterized by m features
298 $\{a_1, a_2, \dots, a_m\}$.

299 As a first step, we normalize the features in each control group c , so that their
300 value lies in $[0,1]$.

$$a'_{i,j} = \frac{a_{i,j} - \min(\{a|a \in A_j\})}{\max(\{a|a \in A_j\}) - \min(\{a|a \in A_j\})}, \quad (1)$$

301 where $a_{i,j}$ represents feature j of the sample i in the control group X_c , and A_j are all
302 values of feature j in the control group X_c . Each sample q_i is thus represented as a
303 feature vector of normalized features $q_i = (a'_{i,1}, a'_{i,2}, \dots, a'_{i,m})$. To estimate the local
304 sample density around a particular point q_i in X_c , we define a subset $N_{q_i} \subseteq X_c$ such
305 that it contains the k points $x' \in X_c$ which are the closest to q_i . Distance D is measured
306 using the Euclidean distance. We define $\text{Dist}(q_i, X_c) = \{D(q_i, x') \mid x' \in X_c\}$ as the set
307 of all distances from q_i to points in X_c . After sorting the points in $\text{Dist}(q_i, X_c)$ into
308 a tuple (d_1, d_2, \dots, d_n) , where $(d_1 \leq d_2 \leq \dots \leq d_n)$, the k nearest neighbors are the
309 first k elements.

310 Next, we quantify the local sample density λ of q_i as the inverse of the sum of the
311 distance to its k nearest neighbors in control group c .

$$\lambda(q_i, c) = \frac{1}{\sum_{x' \in N_{q_i}} D(q_i, x')} \quad (2)$$

312 For each individual q_i in each of the control groups containing n samples,
313 respectively, we calculate the local sample densities λ as described above.

$$\Lambda_c = \{\lambda(q_i, c) \mid i = 1, 2, \dots, n\}, \quad (3)$$

314 To ensure comparability between the different control groups, we divide the local
315 densities by the control-group specific median.

$$\lambda'(q_i, c) = \frac{\lambda(q_i, c)}{\text{median}(\Lambda_c)} \quad (4)$$

316 As a result we have a set of normalized local sample density estimations for all of the
317 g control groups $\Lambda' = \{\Lambda'_1, \Lambda'_2, \dots, \Lambda'_g\}$.

318 We introduce context to the local sample density estimations and analyze their
319 distribution across all control groups. Due to its flexibility in accommodating various
320 distributive shapes, we use the exponentiated Weibull distribution [60]. The distribu-
321 tion is fitted on all normalized local sample density estimation in Λ' . Using the fitted
322 distribution, we derive the likelihood of a normalized local sample density estimation.

$$f(x, b, d) = bd[1 - \exp(-x^d)]^{b-1} \exp(-x^d)x^{d-1}, \quad (5)$$

323 where $x = \lambda'(q_i, c)$ is the normalized local density value of sample q_i in control
324 group c , b is the exponentiation parameter, and d is the shape parameter of the
325 non-exponentiated Weibull law.

326 We use the fitted distribution f to convert all local sample density estimations
 327 $\lambda'(q_i, c)$ into measures of likelihood. To keep as much information as possible, we add a
 328 sign to f , which indicates in which direction a sample is deviating from the median. In
 329 this context, samples whose local sample density is smaller than the medium, receive
 330 a negative value, while samples whose local sample density is larger than the medium,
 331 have a positive value.

$$f^*(x) = \begin{cases} -f(x, b, d) & \text{if } x < 1, \\ f(x, b, d) & \text{otherwise} \end{cases} \quad (6)$$

332 Finally, to foster intuitive interpretation, we scale the signed likelihood f^* to an
 333 interval of $[-1, 1]$, where -1 indicates lowest sample density found and 1 indicates
 334 maximal sample density found.

$$f^{**}(x) = 2 * \frac{f^*(x) - \min(\{f^*(q|q \in X)\})}{\max(\{f^*(q|q \in X)\}) - \min(\{f^*(q|q \in X)\})} - 1 \quad (7)$$

335 The final value f^{**} is a normativity estimation on how common the sample q_i appears
 336 within a particular control group c , measured by its local sample density λ' .

337 5.1.2 Normativity Profile

338 To create a normativity profile for an individual sample q_i , several normativity estima-
 339 tions in different, not mutually exclusive, control groups can be combined, evaluating
 340 the commonness of an individual measurement from multiple meaningful angles or
 341 viewpoints.

$$\phi_i = \{f^{**}(\lambda'(q_i, c_1)), f^{**}(\lambda'(q_i, c_2)), \dots, f^{**}(\lambda'(q_i, c_g))\} \quad (8)$$

342 5.1.3 Meta Normativity

343 To synthesize the comprehensive information entailed in an individual normativity
 344 profile ϕ_i into a single, actionable metric, we conduct a second layer of normativity
 345 estimation (meta-normativity).

346 Basis to this is the first layer of normativity estimation, in which the local density
 347 estimation algorithm described in section 5.1.1 is applied to medical data of a popula-
 348 tion or study sample. In this step, the local sample density estimation is based on the
 349 m medical data features. Using the algorithm outputs, a normativity profile ϕ_i can
 350 be generated for each individual. The normativity profile expresses how common the
 351 medical observations are in relation to the samples contained in each control group.

352 In the second layer of normativity estimation, we use the normativity profile ϕ_i as
 353 input data and repeat the local sample density estimation approach. Now, the local
 354 density estimation algorithm is using the g normativity measures of ϕ as features.
 355 Thereby, we measure the commonness of a normativity profile in relation to other
 356 normativity profiles seen a particular reference population. This can either be done
 357 globally (on all normativity profiles of the sample), or again in in tailored control

358 groups (evaluating the commonness of a normativity profile with respect to a par-
359 ticular sample subpopulation). The output of this meta-normativity estimation is the
360 return value of the N^3 algorithm, what we call the N^3 marker.

$$N^3 = f^{**}(\lambda'(\phi_i, c)) \quad (9)$$

361 5.1.4 Training vs. Inference Phase

362 The N^3 algorithm is trained using a normative reference sample X . There are two sub-
363 sequent layers of local density estimation. The first layer operates on the algorithm's
364 input data. During the process, scaling parameters for the input features, as well as
365 the median local sample density are derived and persisted per control group, respec-
366 tively. Also, the parameters of the fitted probability density function and the final
367 scaling function are persisted. Afterwards, all samples in X undergo the normativity
368 evaluations and are expressed in individual normativity profiles $\Phi = \{\phi_1, \phi_2, \dots, \phi_n\}$
369 (see Equation 8).

370 Using the resulting normativity profiles of the normative reference sample Φ as
371 input, a second layer of normativity estimation is applied. This time, the individual
372 normativity profiles ϕ_i are subject to local sample density estimation ($\lambda'(\phi_i, c)$). Again,
373 the scaling parameters as well as the median local sample density are persisted per
374 control group, respectively. Control groups may now be different than those in the
375 first stage. Finally, another probability density function is fitted, this time on the local
376 sample densities of Φ . Again, the fitting parameters as well as those of the scaling
377 function are persisted.

378 During inference time, a novel sample p is evaluated in relation to the controls
379 groups C of training sample X . For each control group, the feature values of p are scaled
380 according to the parameters persisted during training, and the k nearest neighbors
381 of p are determined, respectively. We calculate $f^{**}(\lambda'(p, c))$ in relation to samples
382 seen in X_c . After applying the first layer of local sample density estimation, several
383 normativity evaluations in different control groups are summarized in a normativity
384 profile ϕ_p . In the second step, the normativity profile ϕ_p is evaluated in relation to the
385 normativity profiles seen in the reference sample (Φ), using the parameters persisted
386 during the second stage of training. The final output is derived by $N_p^3 = f^{**}(\lambda'(\phi_p, c))$

387 5.1.5 Application to Brain Structure

388 In our application to brain structure, we stratify the training sample by sex and age,
389 resulting into 100 control groups containing same-aged females or males (22 to 72
390 years), respectively. Each sample is characterized by 5 different features, namely the
391 brain structural volumes (GM, WM, WMH, CSF, TIV) of each individual. To miti-
392 gate different sample sizes of different age groups, we join either the lower, the upper,
393 or both neighboring age groups of underrepresented age groups, so that the sample
394 size per age group approximates the median sample size available per sex. We set the
395 k parameter to 10% of the control group sample size, but limit its upper bound to
396 15 to prevent too broad comparisons $k = \min(\text{round}(0.1 \times n), 15)$. Applying the N^3
397 algorithm, we then first evaluate the commonness of an individual brain structure in
398 comparison to all available age groups of the same sex. The result are normativity

399 profiles, indicating the alignment of the brain structure in relation to the reference
400 samples seen across the aging continuum. In the next step, we use all normativity pro-
401 files (across genders) and evaluate their normativity in relation to other representative
402 samples of the same chronological age. The final N³ marker indicates how common a
403 brain structural normativity profile is in the chronological age group of the individual.

404 5.2 Materials

405 Neuroimaging data from six different studies were provided by the respective con-
406 sortia. Our study includes data from the German National Cohort (NAKO)[61–63],
407 the Alzheimer’s Disease Neuroimaging Initiative (ADNI) [64], the Münster-Marburg
408 Affective Disorder Cohort (MACS) [65], the Australian Imaging, Biomarker Lifestyle
409 Study of Aging (AIBL) [66], the Frontotemporal Lobar Degeneration Neuroimaging
410 Initiative (NIFD), and the Open Access Series of Imaging Studies 3 (OASIS3) [67, 68].
411 We give a short overview of our approach to integrate these resources in our analyses,
412 before we introduce each study population in detail below.

413 5.2.1 Training and Test Data

414 In general, if more than one measurement was available per participant, we restrict
415 each study’s dataset to the first (baseline) measurement of the participant. Exclusion
416 criteria were applied based on age; participants younger than 22 years or older than
417 72 were omitted from the study, due to insufficient sample sizes in the normative
418 reference sample. All neuroimaging data utilized in this study were T1-weighted MRI
419 scans from these baseline measurements. These images underwent preprocessing using
420 the standard software CAT12 (version: cjp_v0008, spm12 build v7771; cat12 build
421 r1720) default parameters. In short, images were bias-corrected, tissue classified, and
422 normalized to MNI-space using linear and non-linear transformations. Subsequently,
423 the derived GM, WM, WMH, CSF, and TIV volumes were extracted.

424 *Training Data*

425 The training data for fitting models of the different normative modeling approaches
426 comprised 30,047 samples from the population-based NAKO cohort (for details see
427 below). We exclude age groups below 22 years and above 72 years due to small sample
428 sizes (n < 100), which restricts the final sample to 29,883. We then fit the models of
429 the different normative model approaches using this large and diverse sample.

430 *Test Data*

431 To investigate each normativity marker’s effectiveness in identifying brain structural
432 anomalies and (early) signs of neurodegeneration, additional data involving 5,857
433 participants were utilized, sourced from ADNI, AIBL, OASIS and NIFD datasets
434 (for details see section 5.2.2). The collective samples include cognitively unimpaired
435 individuals as well as those diagnosed with Mild Cognitive Impairment, Alzheimer’s
436 Disease and Frontotemporal Dementia.

437 ***Data for Stability Analysis***

438 Finally, to evaluate the robustness of the N³ brain structural normativity assessments,
439 we use artificially downsampled subgroups of the NAKO study for training. Validation
440 subsets included n=835 healthy control participants from the MACS study which
441 predominantly comprises younger and middle-aged adults, and an additional n=1073
442 healthy older adults from the ADNI study to span a wider age demographic (see
443 Methods section 5.5).

444 **5.2.2 Study Populations**

445 ***German National Cohort (NAKO)***

446 The German National Cohort is a population-based longitudinal study initiated in
447 2014 aiming to investigate the risk factors for major chronic diseases in 200,000 per-
448 sons living in Germany. It contains high-quality neuroimaging data from participants
449 spanning a broad age range. In this study, we utilize the participants' 3.0-Tesla T1w-
450 MPRAGE MRI scans (voxel size 1×1×1 mm³, repetition time/ echo time=2300/2.98,
451 flip angle=9°) [61–63].

452 ***Alzheimer's Disease Neuroimaging Initiative (ADNI)***

453 ADNI is a major multicenter study started in 2003, designed to develop clinical,
454 imaging, genetic, and biochemical biomarkers for the early detection and tracking of
455 Alzheimer's disease. The ADNI was launched as a public-private partnership, led by
456 Principal Investigator Michael W. Weiner, MD. The primary goal of ADNI has been
457 to test whether serial MRI, positron emission tomography (PET), other biological
458 markers, and clinical and neuropsychological assessment can be combined to measure
459 the progression of neurodegeneration. We included 1.5 and 3.0-Tesla T1w-MPRAGE
460 MRI scans adhering to the ADNI sequence protocol, for scanner specific details
461 please see [https://adni.loni.usc.edu/data-samples/adni-data/neuroimaging/mri/mri-
462 scanner-protocols/](https://adni.loni.usc.edu/data-samples/adni-data/neuroimaging/mri/mri-scanner-protocols/)

463 ***Australian Imaging, Biomarker & Lifestyle Study of Aging (AIBL)***

464 AIBL is an Australian study launched in 2006 focusing on understanding the pathways
465 to Alzheimer's disease. The cohort includes participants diagnosed with Alzheimer's
466 disease, mild cognitive impairment, and cognitively unimpaired elderly participants,
467 providing insights into the aging process and the development of neurodegenerative
468 diseases. AIBL study methodology has been reported previously [69]. MRI scans were
469 performed using a 3D MPRAGE image (voxel size 1.2×1×1 mm³, repetition time/echo
470 time=2300/ 2.98, flip angle=8°)[66].

471 ***NIFD Dataset***

472 The Frontotemporal Lobar Degeneration Neuroimaging Initiative (FTLDNI) was
473 funded through the National Institute of Aging, and started in 2010. The primary
474 goals of FTLDNI were to identify neuroimaging modalities and methods of analy-
475 sis for tracking frontotemporal lobar degeneration (FTLD) and to assess the value
476 of imaging versus other biomarkers in diagnostic roles. The Principal Investigator of

477 NIFD was Dr. Howard Rosen, MD at the University of California, San Francisco. We
478 use the provided 3D MPRAGE T1-weighted images (voxel size $1 \times 1 \times 1$ mm³, repetition
479 time/echo time=2300/2.9, matrix = $240 \times 256 \times 160$) The data are the result
480 of collaborative efforts at three sites in North America. For up-to-date information on
481 participation and protocol, please visit <http://memory.ucsf.edu/research/studies/nifd>

482 ***Open Access Series of Imaging Studies 3 (OASIS3)***

483 OASIS3 serves as a comprehensive digital repository for MRI brain data that supports
484 longitudinal studies of normal aging and cognitive decline [67, 68]. The project is
485 distinguished by its wide age range of participants, providing diverse datasets that
486 enhance the understanding of late-life brain diseases alongside physiological aging
487 processes. We include 3D MPRAGE T1-weighted images (voxel size 1.0 or $1.2 \times 1 \times 1$
488 mm³, repetition time/echo time=2300/2.95 or 2400/3.16 (depending on the scanner),
489 flip angle=9°, FoV=240 or 256mm)

490 ***Marburg-Münster Affective Disorder Cohort Study (MACS)***

491 The MACS cohort is part of the DFG-funded research group FOR2107 cohort,
492 researching the etiology and progression of affective disorders [65]. The goal is to
493 integrate and understand the clinical and neurobiological effects of genetic and envi-
494 ronmental factors, and their complex interactions. Participants received financial
495 compensation and gave written informed consent. We use the T1-weighted neuroimag-
496 ing scans of n=835 healthy control participants to evaluate stability of the N³ models.
497 Images were in Marburg (MR) or Münster (MS) (voxel size $1 \times 1 \times 1$ mm³, repetition
498 time/echo time=MR: 1900, MS: 2130/MR: 2.26, MS: 2.28, flip angle=8°, FoV = 256
499 mm, matrix = 256×256 , slice thickness = 1 mm)

Table 2 Study Data Summary

Study	Group	N Included	Mean Age	Sex
ADNI	HC	1073	68.36 ± 3.3	634 females (59.09%)
	MCI	1529	66.71 ± 4.25	729 females (47.67%)
	AD	588	67.2 ± 4.65	291 females (49.48%)
AIBL	HC	368	68.00 ± 2.77	217 females (58.97%)
	MCI	78	68.05 ± 3.54	33 females (42.31%)
	AD	28	66.89 ± 4.44	16 females (57.14%)
OASIS3	HC	1643	63.36 ± 6.85	1028 females (62.57%)
	MCI	63	66.67 ± 4.85	37 females (58.73%)
	AD	228	66.54 ± 4.94	97 females (42.54%)
NIFD	HC	263	62.71 ± 6.41	148 females (56.27%)
	FTD	317	63.26 ± 5.66	120 females (37.85%)
MACS	HC	835	35.71 ± 12.6	528 females (63.23%)
NAKO	HC	29883	48.45 ± 12.09	13201 females (44.18%)

500 **5.3 Brain Age Model**

501 In the Brain Age paradigm, the brain structure is evaluated with respect to aging
502 effects seen in a healthy reference sample. This is realized by means of a machine

503 learning model trained to predict chronological age from brain structure. The devi-
504 ation between chronological and predicted age is referred to as the Brain Age Gap
505 (BAG). While a small BAG is considered normative and age-appropriate, a larger pos-
506 itive or negative BAG symbolizes premature or delayed neurostructural degeneration,
507 respectively. The resulting normativity estimation, i.e. the BAG values, have been
508 associated with numerous neurological and psychiatric conditions [11, 12]. For com-
509 parison with N³, we train a Brain Age Model using the Python library photonai [70].
510 We use 90% of the available normative dataset for model training. We use a Support
511 Vector Machine (SVM), for which we optimize the C and gamma parameters in the
512 nested-cross-validation procedure (k=10 outer folds and two randomly shuffled inner
513 folds with a test size of 0.1). The best model achieves an average MAE of 5.43. Finally,
514 we use the remaining 10% of the normative training data to train a linear age bias cor-
515 rection as described in Peng et al. [71]. For the evaluation of unseen samples, we use
516 the Brain Age SVM model to predict age and apply the age correction model, before
517 we calculate the difference between the chronological and predicted age, the BAG.

518 5.4 Normative Modeling

519 We calculate normative models on the training data using the Predictive Clinical
520 Neuroscience toolkit as described in Rutherford et al. [22]. To train the models, we
521 normalize GM, WM, WMH, CSF by Total Intracranial Volume (TIV) and fit Bayesian
522 Linear Regression models with default parameters. Subsequently, z-scores for each of
523 the variables are derived, which we aggregate into two normative modeling markers:
524 one being the sum of the absolute z-scores, the second counting the number of absolute
525 z-scores > 1.96.

526 5.5 Statistical Analysis

527 A Type III Sum of Squares ANOVA was performed using an ordinary least squares
528 (OLS) model to assess the discriminative and explanatory power of each normativity
529 marker in distinguishing patients from controls. The model was adjusted for potential
530 confounders, including age, age squared (to mitigate non-linear effects), sex and scan-
531 ner. Partial eta squared (η^2) was used to quantify effect size, providing an estimate
532 of how much variance in disease progression could be explained by each normativity
533 marker, alongside a 95% confidence interval.

534 We evaluate and rank the different normativity markers by post-hoc comparisons of
535 their effect size. To test the observed marker differences for statistical significance, we
536 calculate the ANOVA for each marker with 1000 random permutations. To determine
537 the p value of the marker differences, we evaluate the actual difference between the η^2
538 of our marker N³ and the η^2 of another marker, with those found in the 1000 random
539 permutations.

540 To assess each normativity marker's consistency across age groups, an analysis of
541 age bias was conducted using Spearman's rank correlation to evaluate the correlation
542 between the normativity estimation values and age in healthy controls.

543 To assess stability of the N³ models, the Intraclass Correlation Coefficient (ICC)
544 model (2,1) was applied. For this purpose, we used the NAKO sample to train the

545 normativity models, which were downsampled to mimic smaller study populations.
546 Particularly, we divide the training set in $k=[10, 5, 3, 2]$ non-overlapping parts of equal
547 size, train normativity models within each of these subsets, and use external test data
548 to ensure the stability of the normativity estimates. The stability of the normativity
549 estimates was tested using data from the ADNI and MACS cohort, (see Methods
550 section 5.2.1). To ensure validity of the test, we use only age groups with more than
551 500 samples available from the training sample and more than 20 samples in the test
552 samples.

553 All statistical analyses were implemented in Python using the *scipy*, *statsmodels*
554 and *pingouin* libraries.

555 5.6 Machine Learning Analysis

556 The effectiveness of aging markers in classifying neurodegenerative diseases was fur-
557 ther explored through machine learning techniques. We assessed various performance
558 metrics including balanced accuracy, recall, precision, and F1-score. Our analytical
559 pipeline employed the open-source Python framework photonai [70]. The analysis
560 involved nested cross-validation to robustly estimate model performance and avoid
561 overfitting, using $k=5$ outer folds and $k=10$ inner folds, each fold stratified to entail a
562 balanced proportion of samples from the diseased class. Hyperparameter optimization
563 was performed via Grid Search to fine-tune the support vector machine (SVM) param-
564 eters C and gamma. The machine learning pipeline included steps for z-normalization
565 and balanced sampling (random under-sampling techniques) to address class imbal-
566 ance within the training data. We measure balanced accuracy, recall, precision and
567 f1 score of each of the normativity markers in the classification of neurodegenerative
568 diseases.

Supplementary information.

Acknowledgements. This work was funded by the German Research Foundation (DFG, grant HA7070/2-2, HA7070/3, and HA7070/4 to T.H. and FOR2107 DA1151/5-1, DA1151/5-2, DA1151/9-1, DA1151/10-1, DA1151/11-1 to U.D.; SFB/TRR 393, project grant no 521379614), the Interdisciplinary Center for Clinical Research (IZKF) of the medical faculty of Münster (grant Dan3/022/22 to U.D. and MzH 3/020/20 to T.H.), and the IMF research instrument of the medical faculty of Münster (grant LE 1 1 24 09 to R. Leenings). X. Jiang was supported by the Deutsche Forschungsgemeinschaft (DFG) under Grant CRC 1450—431460824.

This project was conducted with data from the German National Cohort (NAKO) (www.nako.de). The NAKO is funded by the Federal Ministry of Education and Research (BMBF) [project funding reference numbers: 01ER1301A/B/C, 01ER1511D, 01ER1801A/B/C/D and 01ER2301A/B/C], federal states of Germany and the Helmholtz Association, the participating universities and the institutes of the Leibniz Association. We thank all participants who took part in the NAKO study and the staff of this research initiative.

Data collection and sharing for this project was funded by the Alzheimer's Disease Neuroimaging Initiative (ADNI) (National Institutes of Health Grant U01 AG024904) and DOD ADNI (Department of Defense award number W81XWH-12-2-0012). ADNI

is funded by the National Institute on Aging, the National Institute of Biomedical Imaging and Bioengineering, and through generous contributions from the following: AbbVie, Alzheimer's Association; Alzheimer's Drug Discovery Foundation; Araclon Biotech; BioClinica, Inc.; Biogen; Bristol-Myers Squibb Company; CereSpir, Inc.; Cogstate; Eisai Inc.; Elan Pharmaceuticals, Inc.; Eli Lilly and Company; EuroImmun; F. Hoffmann-La Roche Ltd and its affiliated company Genentech, Inc.; Fujirebio; GE Healthcare; IXICO Ltd.; Janssen Alzheimer Immunotherapy Research Development, LLC.; Johnson Johnson Pharmaceutical Research Development LLC.; Lumosity; Lundbeck; Merck Co., Inc.; Meso Scale Diagnostics, LLC.; NeuroRx Research; Neurortrack Technologies; Novartis Pharmaceuticals Corporation; Pfizer Inc.; Piramal Imaging; Servier; Takeda Pharmaceutical Company; and Transition Therapeutics. The Canadian Institutes of Health Research is providing funds to support ADNI clinical sites in Canada. Private sector contributions are facilitated by the Foundation for the National Institutes of Health (www.fnih.org). The grantee organization is the Northern California Institute for Research and Education, and the study is coordinated by the Alzheimer's Therapeutic Research Institute at the University of Southern California. ADNI data are disseminated by the Laboratory for Neuro Imaging at the University of Southern California.

Data was in part provided by OASIS-3: Principal Investigators: T. Benzing, D. Marcus, J. Morris; NIH P50AG00561, P30NS09857781, P01AG026276, P01AG003991, R01AG043434, UL1TR000448, R01EB009352. AV-45 doses were provided by Avid Radiopharmaceuticals, a wholly owned subsidiary of Eli Lilly.

Data collection and sharing for this project was funded by the Frontotemporal Lobar Degeneration Neuroimaging Initiative (National Institutes of Health Grant R01 AG032306). The study is coordinated through the University of California, San Francisco, Memory and Aging Center. FTLDNI data are disseminated by the Laboratory for Neuro Imaging at the University of Southern California. The investigators at NIFD/FTLDNI contributed to the design and implementation of FTLDNI and/or provided data, but did not participate in analysis or writing of this report (unless otherwise listed). The FTLDNI investigators included the following individuals: Howard Rosen; University of California, San Francisco (PI) Bradford C. Dickerson; Harvard Medical School and Massachusetts General Hospital Kimoko Domoto-Reilly; University of Washington School of Medicine David Knopman; Mayo Clinic, Rochester Bradley F. Boeve; Mayo Clinic Rochester Adam L. Boxer; University of California, San Francisco John Kornak; University of California, San Francisco Bruce L. Miller; University of California, San Francisco William W. Seeley; University of California, San Francisco Maria-Luisa Gorno-Tempini; University of California, San Francisco Scott McGinnis; University of California, San Francisco Maria Luisa Mandelli; University of California, San Francisco

Declarations

Data Availability

Data were obtained from the German National Cohort (NAKO), the Alzheimer's Disease Neuroimaging Initiative (ADNI), the Open Access Series of Imaging Studies

3 (OASIS3), the Frontotemporal Lobar Degeneration Neuroimaging Initiative (NIFD), and the Australian Imaging, Biomarker Lifestyle Study of Aging (AIBL). Data of the MACS study are not publicly available. All other data are available upon request via the access management systems of the respective studies. (NAKO: nako.de/forschung, ADNI, AIBL, NIFD: ida.loni.usc.edu, OASIS3: sites.wustl.edu/oasisbrains)

Code Availability

Code to realize the normativity estimation calculations within the N³ framework is written in the Python programming language and is provided as an open-source resource to the scientific community on Github (link tbd).

References

- [1] Stephan, K. E. *et al.* Charting the Landscape of Priority Problems in Psychiatry, Part 1: Classification and Diagnosis. *The Lancet Psychiatry* **3**, 77–83 (2016).
- [2] Bzdok, D. & Meyer-Lindenberg, A. Machine Learning for Precision Psychiatry: Opportunities and Challenges. *Biological Psychiatry: Cognitive Neuroscience and Neuroimaging* **3**, 223–230 (2017).
- [3] Etkin, A. & Mathalon, D. H. Bringing Imaging Biomarkers Into Clinical Reality in Psychiatry. *JAMA Psychiatry* **81**, 1142–1147 (2024).
- [4] Woo, C.-W., Chang, L. J., Lindquist, M. A. & Wager, T. D. Building better biomarkers: brain models in translational neuroimaging. *Nature Neuroscience* **20**, 365–377 (2017).
- [5] Yatham, L. N. Biomarkers for clinical use in psychiatry: where are we and will we ever get there? *World Psychiatry* **22**, 263–264 (2023).
- [6] Abi-Dargham, A. *et al.* Candidate biomarkers in psychiatric disorders: state of the field. *World Psychiatry* **22**, 236–262 (2023).
- [7] Collins, F. S. & Harold, V. A New Initiative on Precision Medicine. *New England Journal of Medicine* **372**, 793–795 (2015).
- [8] Khoury, M. J., Iademarco, M. F. & Riley, W. T. Precision Public Health for the Era of Precision Medicine. *American Journal of Preventive Medicine* **50**, 398–401 (2016).
- [9] Franke, K. & Gaser, C. Ten Years of BrainAGE as a Neuroimaging Biomarker of Brain Aging: What Insights Have We Gained? *Frontiers in Neurology* **10**, 789 (2019).
- [10] Cole, J. H. & Franke, K. Predicting Age Using Neuroimaging: Innovative Brain Ageing Biomarkers. *Trends in Neurosciences* **40**, 681–690 (2017).
- [11] Baecker, L., Garcia-Dias, R., Vieira, S., Scarpazza, C. & Mechelli, A. Machine learning for brain age prediction: Introduction to methods and clinical applications. *EBioMedicine* **72**, 103600 (2021).
- [12] Cole, J. H. Multimodality neuroimaging brain-age in UK biobank: relationship to biomedical, lifestyle, and cognitive factors. *Neurobiology of Aging* **92**, 34–42 (2020).
- [13] Biondo, F. *et al.* Brain-age is associated with progression to dementia in memory clinic patients. *NeuroImage: Clinical* **36**, 103175 (2022).

- [14] Lee, J. *et al.* Deep learning-based brain age prediction in normal aging and dementia. *Nature Aging* **2**, 412–424 (2022).
- [15] Zhao, L. *et al.* Morphological and genetic decoding shows heterogeneous patterns of brain aging in chronic musculoskeletal pain. *Nature Mental Health* **2**, 435–449 (2024).
- [16] Elliott, M. L. MRI-based biomarkers of accelerated aging and dementia risk in midlife: how close are we? *Ageing Research Reviews* **61**, 101075 (2020).
- [17] Dong, A. *et al.* Heterogeneity of neuroanatomical patterns in prodromal Alzheimer's disease: links to cognition, progression and biomarkers. *Brain* **140**, 735–747 (2017).
- [18] Jagust, W. J. Youthfulness begins in youth. *Nature Aging* **1**, 239–240 (2021).
- [19] Tian, Y. E., Cole, J. H., Bullmore, E. T. & Zalesky, A. Brain, lifestyle and environmental pathways linking physical and mental health. *Nature Mental Health* **2**, 1250–1261 (2024).
- [20] Bartrés-Faz, D. *et al.* Psychological profiles associated with mental, cognitive and brain health in middle-aged and older adults. *Nature Mental Health* **3**, 92–103 (2025).
- [21] Marquand, A. F., Rezek, I., Buitelaar, J. & Beckmann, C. F. Understanding Heterogeneity in Clinical Cohorts Using Normative Models: Beyond Case-Control Studies. *Biological Psychiatry* **80**, 552–561 (2016).
- [22] Rutherford, S. *et al.* The normative modeling framework for computational psychiatry. *Nature Protocols* **17**, 1711–1734 (2022).
- [23] Rutherford, S. *et al.* Evidence for embracing normative modeling. *eLife* **12**, e85082 (2023).
- [24] Segal, A. *et al.* Embracing variability in the search for biological mechanisms of psychiatric illness. *Trends in Cognitive Sciences* (2024).
- [25] Cover, T. & Hart, P. Nearest neighbor pattern classification. *IEEE Transactions on Information Theory* **13**, 21–27 (1967).
- [26] Bethlehem, R. A. I. *et al.* Brain charts for the human lifespan. *Nature* **604**, 525–533 (2022).
- [27] Bzdok, D., Altman, N. & Krzywinski, M. Statistics versus machine learning. *Nature Methods* **15**, 233–234 (2018).
- [28] Poldrack, R. A., Huckins, G. & Varoquaux, G. Establishment of Best Practices for Evidence for Prediction. *JAMA Psychiatry* **77**, 534–540 (2020).

- [29] Tan, Y. Y. *et al.* Comparing clinical trial population representativeness to real-world populations: an external validity analysis encompassing 43895 trials and 5685738 individuals across 989 unique drugs and 286 conditions in England. *The Lancet Healthy Longevity* **3**, e674–e689 (2022).
- [30] Spall, H. G. C. V., Toren, A., Kiss, A. & Fowler, R. A. Eligibility Criteria of Randomized Controlled Trials Published in High-Impact General Medical Journals: A Systematic Sampling Review. *JAMA* **297**, 1233–1240 (2007).
- [31] Abid, A., Zhang, M. J., Bagaria, V. K. & Zou, J. Exploring patterns enriched in a dataset with contrastive principal component analysis. *Nature Communications* **9**, 2134 (2018).
- [32] Halder, R. K., Uddin, M. N., Uddin, M. A., Aryal, S. & Khraisat, A. Enhancing K-nearest neighbor algorithm: a comprehensive review and performance analysis of modifications. *Journal of Big Data* **11**, 113 (2024).
- [33] Belle, A. *et al.* Big Data Analytics in Healthcare. *BioMed Research International* **2015**, 370194 (2015).
- [34] Ghassemi, M. *et al.* A Review of Challenges and Opportunities in Machine Learning for Health. *AMIA Joint Summits on Translational Science proceedings. AMIA Joint Summits on Translational Science* **2020**, 191–200 (2020).
- [35] Xuan, Y. *et al.* Standardization and harmonization of distributed multi-center proteotype analysis supporting precision medicine studies. *Nature Communications* **11**, 5248 (2020).
- [36] Froelicher, D. *et al.* Truly privacy-preserving federated analytics for precision medicine with multiparty homomorphic encryption. *Nature Communications* **12**, 5910 (2021).
- [37] Zhang, Y. & Chung, Y. Nonparametric estimation of linear personalized diagnostics rules via efficient grid algorithm. *Statistics in Medicine* **43**, 1354–1371 (2024).
- [38] Oh, S. S. *et al.* Diversity in Clinical and Biomedical Research: A Promise Yet to Be Fulfilled. *PLoS Medicine* **12**, e1001918 (2015).
- [39] Hood, L., Lovejoy, J. C. & Price, N. D. Integrating big data and actionable health coaching to optimize wellness. *BMC Medicine* **13**, 4 (2015).
- [40] Bodicoat, D. H. *et al.* Promoting inclusion in clinical trials—a rapid review of the literature and recommendations for action. *Trials* **22**, 880 (2021).
- [41] Elhussein, A. *et al.* A framework for sharing of clinical and genetic data for precision medicine applications. *Nature Medicine* 1–12 (2024).

- [42] Meehan, A. J. *et al.* Clinical Prediction Models in Psychiatry: A Systematic Review of Two Decades of Progress and Challenges. *Molecular Psychiatry* **1**–9 (2022).
- [43] Wrigglesworth, J. *et al.* Factors associated with brain ageing - a systematic review. *BMC Neurology* **21**, 312 (2021).
- [44] Gafson, A. R. *et al.* Neurofilaments: neurobiological foundations for biomarker applications. *Brain* **143**, 1975–1998 (2020).
- [45] Braak, H. & Braak, E. Neuropathological stageing of Alzheimer-related changes. *Acta Neuropathologica* **82**, 239–259 (1991).
- [46] Wilson, D. M. *et al.* Hallmarks of neurodegenerative diseases. *Cell* **186**, 693–714 (2023).
- [47] Skampardoni, I. *et al.* Genetic and Clinical Correlates of AI-Based Brain Aging Patterns in Cognitively Unimpaired Individuals. *JAMA Psychiatry* **81**, 456–467 (2024).
- [48] Finch, C. E. & Crimmins, E. M. Inflammatory Exposure and Historical Changes in Human Life-Spans. *Science* **305**, 1736–1739 (2004).
- [49] Gillman, M. W. Developmental Origins of Health and Disease. *The New England Journal of Medicine* **353**, 1848–1850 (2005).
- [50] Dehnel, T. The European Dementia Prevention Initiative. *The Lancet Neurology* **12**, 227–228 (2013).
- [51] Flier, W. M. v. d., Vugt, M. E. d., Smets, E. M. A., Blom, M. & Teunissen, C. E. Towards a future where Alzheimer's disease pathology is stopped before the onset of dementia. *Nature Aging* **3**, 494–505 (2023).
- [52] Yang, Z. *et al.* Brain aging patterns in a large and diverse cohort of 49,482 individuals. *Nature Medicine* 1–12 (2024).
- [53] Yu, M., Sporns, O. & Saykin, A. J. The human connectome in Alzheimer disease — relationship to biomarkers and genetics. *Nature Reviews Neurology* **17**, 545–563 (2021).
- [54] Prabhakar, C. *et al.* ViT-AE++: Improving Vision Transformer Autoencoder for Self-supervised Medical Image Representations. *arXiv* (2023).
- [55] Shen, L. & Thompson, P. M. Brain Imaging Genomics: Integrated Analysis and Machine Learning. *Proceedings of the IEEE* **108**, 125–162 (2020).
- [56] Tozzi, L. *et al.* Personalized brain circuit scores identify clinically distinct biotypes in depression and anxiety. *Nature Medicine* **30**, 2076–2087 (2024).

- [57] Blume, H. Neurodiversity - On the neurological underpinnings of geekdom. *The Atlantic* (1998). URL <https://www.theatlantic.com/magazine/archive/1998/09/neurodiversity/305909/>.
- [58] Ortega, F. The Cerebral Subject and the Challenge of Neurodiversity. *BioSocieties* **4**, 425–445 (2009).
- [59] Dwyer, P. The Neurodiversity Approach(es): What Are They and What Do They Mean for Researchers? *Human Development* **66**, 73–92 (2022).
- [60] Mudholkar, G. & Srivastava, D. Exponentiated Weibull family for analyzing bathtub failure-rate data. *IEEE Transactions on Reliability* **42**, 299–302 (1993).
- [61] Peters, A. *et al.* Framework and baseline examination of the German National Cohort (NAKO). *European Journal of Epidemiology* **37**, 1107–1124 (2022).
- [62] Consortium, G. N. C. G. The German National Cohort: aims, study design and organization. *European Journal of Epidemiology* **29**, 371–382 (2014).
- [63] Bamberg, F. *et al.* Whole-Body MR Imaging in the German National Cohort: Rationale, Design, and Technical Background. *Radiology* **277**, 206–220 (2015).
- [64] Petersen, R. C. *et al.* Alzheimer’s Disease Neuroimaging Initiative (ADNI) Clinical characterization. *Neurology* **74**, 201–209 (2010).
- [65] Vogelbacher, C. *et al.* The Marburg-Münster Affective Disorders Cohort Study (MACS): A Quality Assurance Protocol for MR Neuroimaging Data. *NeuroImage* **172**, 450–460 (2018).
- [66] Fowler, C. *et al.* Fifteen Years of the Australian Imaging, Biomarkers and Lifestyle (AIBL) Study: Progress and Observations from 2,359 Older Adults Spanning the Spectrum from Cognitive Normality to Alzheimer’s Disease. *Journal of Alzheimer’s Disease Reports* **5**, 443–468 (2021).
- [67] Marcus, D. S. *et al.* Open Access Series of Imaging Studies (OASIS): Cross-sectional MRI Data in Young, Middle Aged, Nondemented, and Demented Older Adults. *Journal of Cognitive Neuroscience* **19**, 1498–1507 (2007).
- [68] LaMontagne, P. J. *et al.* OASIS-3: Longitudinal Neuroimaging, Clinical, and Cognitive Dataset for Normal Aging and Alzheimer Disease. *medRxiv* 2019.12.13.19014902 (2019).
- [69] Ellis, K. A. *et al.* The Australian Imaging, Biomarkers and Lifestyle (AIBL) study of aging: methodology and baseline characteristics of 1112 individuals recruited for a longitudinal study of Alzheimer’s disease. *International Psychogeriatrics* **21**, 672–687 (2009).

- [70] Leenings, R. *et al.* PHOTONAI—A Python API for Rapid Machine Learning Model Development. *PLoS ONE* **16**, e0254062 (2021).
- [71] Peng, H., Gong, W., Beckmann, C. F., Vedaldi, A. & Smith, S. M. Accurate brain age prediction with lightweight deep neural networks. *Medical Image Analysis* **68**, 101871 (2021).